Available online at www.sciencedirect.com
ScienceDirect
Journal of Theoretical Biology 242 (2006) 464–477
Journal of Theoretical Biology
www.elsevier.com/locate/yjtbi

Probing the effects of the well-mixed assumption on viral infection dynamics

Catherine Beauchemin*

Department of Physics, University of Alberta, Edmonton, AB, Canada T6G 2J1

Received 23 May 2005; received in revised form 19 March 2006; accepted 20 March 2006
Available online 2 May 2006

Abstract

Viral kinetics have been extensively studied in the past through the use of spatially well-mixed ordinary differential equations describing the time evolution of the diseased state. However, emerging spatial structures such as localized populations of dead cells might adversely affect the spread of infection, similar to the manner in which a counter-fire can stop a forest fire from spreading. In a previous publication [Beauchemin, C., Samuel, J., Tuszynski, J., 2005. A simple cellular automaton model for influenza A viral infections. J. Theor. Biol. 232(2), 223–234], a simple two-dimensional cellular automaton model was introduced and shown to be accurate enough to model an uncomplicated infection with influenza A. Here, this model is used to investigate the effects of relaxing the well-mixed assumption. Particularly, the effects of the initial distribution of infected cells, the regeneration rule for dead epithelial cells, and the proliferation rule for immune cells are explored and shown to have an important impact on the development and outcome of the viral infection in our model.

Keywords: Cellular automaton; Agent-based models; Individual-based models; Viral infection dynamics; Spatial heterogeneity; Mathematical modelling; Well-mixed assumption

1. Introduction

Mathematical modelling of viral infection dynamics has become a very popular approach to understanding and characterizing the dynamics of viral infections. The basic viral infection model, which was introduced by Perelson et al. (1996) and Perelson (2002), namely

$$\frac{dT}{dt} = \lambda - dT - kTV, \tag{1}$$

$$\frac{dI}{dt} = kTV - \delta I, \tag{2}$$

$$\frac{dV}{dt} = pI - cV, \tag{3}$$

describes the temporal evolution of the population of susceptible or target cells, T, which become infected, I, as a result of their interactions with virus particles, V. This model is widely used with minor or major modifications to study the dynamics of various viral infections. Typically, these mathematical modelling efforts seek to determine crucial parameters of the dynamics of a specific viral infection which would be impractical or arduous to extract experimentally.

But those simple ordinary differential equation (ODE) models make the very important assumption that the various populations of cells and virions are uniformly distributed over the space where the infection takes place for all times; an assumption that is rarely realistic, and which may or may not affect in a significant way the resulting dynamics. For this reason, there is growing interest in probing the effect of spatial distribution on systems in ecology (Durrett, 1994; Durrett and Levin, 1994; Young et al., 2001), epidemiology (Lloyd and May, 1996; Hagenaars et al., 2004) and immunology (Funk et al., 2005; Louzoun et al., 2001; Strain et al., 2002).

Here, I explore the effects of spatial structures on the dynamics of a viral infection, whose target cells are fixed in space, using a two-dimensional cellular automaton introduced in previous work (Beauchemin et al., 2005). I will

*Tel.: +1 819 777 2279; fax: +1 505 277 6927.
E-mail address: cbeau@cs.unm.edu.

0022-5193/$ - see front matter © 2006 Elsevier Ltd. All rights reserved.
doi:10.1016/j.jtbi.2006.03.014

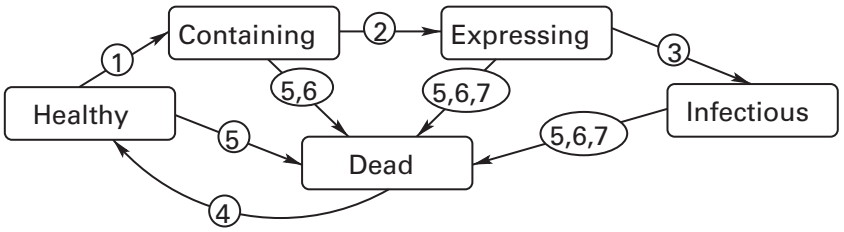

(1) Healthy epithelial cells get infected at rate $\beta/8 = 0{:}25\ \mathrm{h}^{-1}$ per infectious Moore neighbour (8 nearest neighbours), where $\beta = 2\ \mathrm{h}^{-1}$ is the rate of infection of neighbours by infectious cells.
(2) A cell containing virions and which has been infected for $\tau_E = 4$ h begins expressing the viral peptide on their epitope.
(3) An expressing cell that has been infected for $\tau_I = 6$ h becomes infectious.
(4) A dead cell is replaced by a healthy cell at rate $b^{-1} \times$ # healthy / # dead, where $b = 12$ h is the division time of an epithelial cell.
(5) All cells will die of old age after living for exactly $\delta_H = 380$ h, unless they die earlier because of viral toxicity or immune recognition (see below).
(6) Because of viral toxicity, infected cells (i.e. containing + expressing + infectious) will die after having been infected for $\delta_I = 24$ h,unless they die earlier from recognition (see below) or from old age (see above).
(7) Finally, expressing and infectious cells die when "recognized" by an activated immune cell.

Box 1. Evolution rules for the epithelial cells in the cellular automaton model.

explore which kind of effects spatial structures can have on the evolution and outcome of a spatially localized viral infection. I will also show how these spatial structures emerge and by which process they affect the dynamics of the infection.

In the next section the reader will briefly be reminded about the rules and parameters of the cellular automaton model. Then, in Section 3, the effect of the distribution of initially infected cells on the progression of the infection is investigated. Section 4 compares a local regeneration rule for epithelial cells to a global rule, i.e. the rule for the replacement of dead epithelial cells with healthy cells. In Section 5, the effects of the addition of immune cells at random locations versus addition at the site of recruitment are explored. Finally, in Section 6, the significance of the spatial effects in the particular case of an uncomplicated influenza A viral infection is discussed.

2. The cellular automaton

The cellular automaton (CA) model that will be used in this work was introduced in Beauchemin et al. (2005), where the values chosen for each parameter are justified, and the choice of boundary conditions and grid size were shown to be safe. The relationship between the notation used here and that of Beauchemin et al. (2005) is listed in Appendix A. The model was implemented in C as a client simulation for the MASyV package (Beauchemin, 2005). It considers two species of cells: epithelial cells which are the target of the viral infection and immune cells which fight the infection. The CA is run on a two-dimensional square lattice where each site represents one epithelial cell, and immune cells are mobile, moving from one lattice site (epithelial cell) to another. The simulation grid is updated synchronously and has toroidal boundary conditions for both cell types.[1] The virus particles are not explicitly considered, rather the infection is modelled as spreading directly from one epithelial cell to another.

The evolution rules of the CA model for the epithelial and immune cell species are enumerated in Boxes 1 and 2, respectively. At initialization time, each epithelial cell is assigned a random age between 0 and δ_H. All but a fraction $\rho_C = 0.01$ epithelial cells are initialized as healthy, the rest are set as containing virions. Additionally, $\rho_M = 1.5 \times 10^{-4}$ unactivated immune cells per epithelial cell are placed at random locations on the grid.

3. Distribution of initially infected cells

In our CA model, the parameter ρ_C is the fraction of epithelial cells initially set in the infected state, and its default value is 1%. In Beauchemin et al. (2005), the cells to be initially set to the infected state were picked at

[1]Note that the use of asynchronous updating, whereby individual cells were sequentially picked at random and updated, has been tested and resulted in a statistically identical behaviour (agreement within one standard deviation).

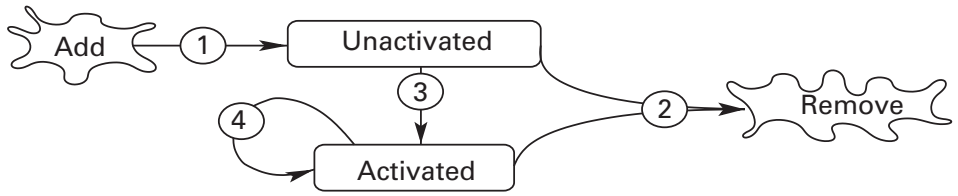

(1) Unactivated immune cells are added at random lattice sites as needed to maintain a minimum density of $\rho_M = 1.5 \times 10^{-4}$ unactivated immune cells per epithelial cell.
(2) All immune cells die of old age after living for exactly $\delta_M = 168$ h.
(3) An unactivated immune cell becomes activated when it first occupies an expressing or infectious lattice site.
(4) If an activated cell is occupying an expressing or infectious lattice site, it kills the epithelial cell and $r_M = 0.25$ new activated immune cells are added at random locations on the grid. The integer part of r_M (if $r_M > 1$) is used to determine the number of immune cells that will be added and the fractional part is taken to be the probability of adding an additional immune cell.

Additionally, immune cells move randomly on the CA lattice at a speed of one lattice site per time step, and there are $v = 6$ time steps /h.

Box 2. Evolution rules for the immune cells in the cellular automaton model.

random and this resulted in single infected cells as well as groupings or patches of neighbouring infected cells of various sizes. One way to investigate the effect of spatial heterogeneities on the dynamics of the infection is to change the spatial configuration of the epithelial cells that are initially set in the infected state. To do this, our model was modified to distribute the initially infected cells into groups or patches of fixed size so that the effect of the size of the patches of infected cells on the dynamics of the infection can be investigated.

A new parameter, s, is added to our CA model, being the number of cells that make up a patch of initially infected cells. Since the number of epithelial cells to be initially infected is not necessarily divisible by s, the quotient of that division gives the number of patches to be added to the simulation grid at start up, and the remainder of the division is used to set the probability that an extra patch of size s be added. This means that a fixed initial patch size is enforced at the expense of a fixed fraction of initially infected cells. Each patch of infected cells is individually constructed and is added at a random location on the grid, ensuring that no two patches are in contact with each other. The Beauchemin et al. (2005) CA model defines the neighbourhood of a site as consisting of the site itself and its eight closest sites (Moore neighbourhood). A patch of s infected cells is constructed by starting with a seed site and growing it by sequentially picking one site at random from the set of sites that neighbour previously selected sites. Note that this method of forming patches results in patches with densities that decrease with increasing distance from the centre. This characteristic is consistent with a splatter or spray of virions and thus this method was preferred over other patch growing methods such as diffusion-limited aggregation, and random walk additions around a seed.

The results for patches ranging in size from 1 to 1232 infected cells are presented in Fig. 1. One can see that increasing initial patch sizes result in fewer infected cells and less epithelial damage. This is not surprising since only the cells that make up the perimeter of the patch, i.e. those that have healthy neighbours, can infect other cells. As patches grow, their perimeter to area ratio, namely the fraction of infectious cells that have healthy neighbours, will decrease and so will the effective infection rate.

Let us illustrate this by an example. Consider a system where infected cells infect all of their uninfected Moore neighbours (eight nearest neighbours) in each time step (an infection rate of 100%). The evolution of the system from an initial single seed is illustrated in Fig. 2. From the relation derived in the table of Fig. 2, one can compute the effective infection rate, i.e. the number of newly infected cells per infected cell at time step n, to be $8(n+1)/(2n+1)^2 = 4/\sqrt{I} + 4/I$, where $I = (2n+1)^2$ is the number of infected cells in a square patch after n time steps. A graph of the effective infection rate as a function of the number of infected cells in a square patch is presented in Fig. 3. For this toy model, the effective infection rate is proportional to $1/\sqrt{I}$ for $I \gg 1$.

Another interesting feature that can be seen in Fig. 1 is the increasing standard deviation for increasing initial patch sizes. This is easily explained with the fact that the larger the parameter s, the fewer the sites of infection. In other words, as the initial patch size increases, the 50 simulations are averaging over fewer infection sites. Fig. 4 presents two example simulations to illustrate the differences that can arise between simulations produced using

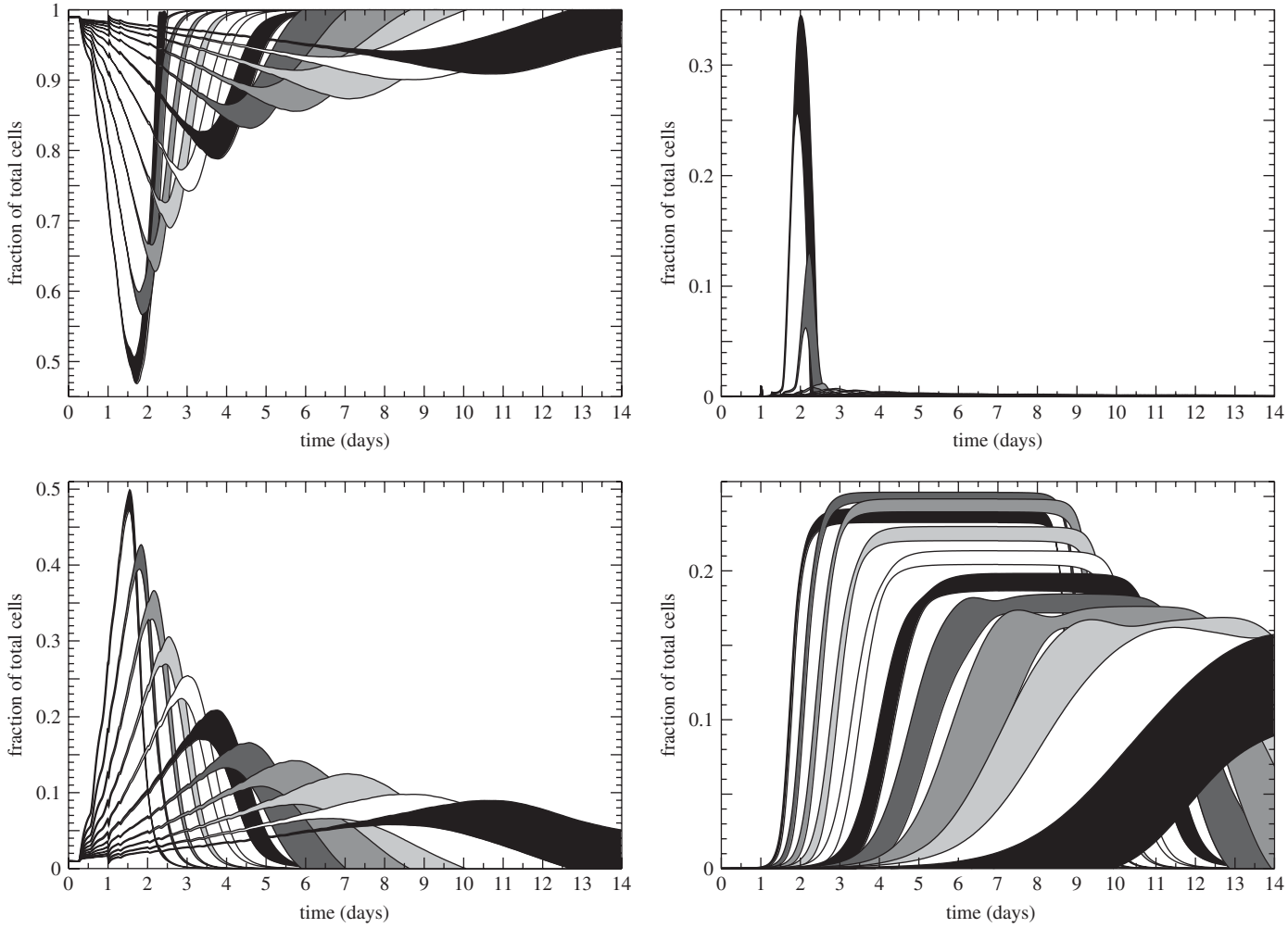

Fig. 1. The effect of varying the initial patch size, s, on the dynamics of the viral infection. The graphs show the time evolution of the populations of healthy (top left), dead (top right), infected (bottom left), and immune cells (bottom right) for s values of 1, 2, 4, 8, 16, 35, 77, 154, 308, 616, and 1232 cells. The greyed areas mark one standard deviation after 50 runs for each initial patch size, with periodically decreasing darkness corresponding to increasing initial patch sizes. In all cases, the black band that peaks first is $s = 1$. The graphs show that the dynamics of the viral infection is sensitive to the spatial organization of the initially infected epithelial cells.

the same parameter values, when the initial patch size is large. In the case of the example simulations presented in Fig. 4, early detection made the difference between a small and short infection, and a longer infection resulting in a greater number of infected and dead cells. The larger the initial patch size, the fewer the number of infected patches and thus, the more pronounced this effect will be. This variability for larger values of s can be reduced by averaging simulations with the same number of infection sites (same number of patches) rather than the same absolute number of infected cells (same area).

Finally, it can be seen that there is a decrease in peak immune cell concentration for initial patch sizes below $s = 2$. It is clear that there are two processes at work: one which dominates at small initial patch sizes and one which dominates at large initial patch sizes. As seen in the bottom left of Fig. 1, the peak number of infected cells decreases monotonically as the initial patch size is increased. The peak concentration of immune cells is, mostly, determined by the peak number of infected cells, and this explains the decrease in the peak concentration of immune cells as the patch size increases. However, I have yet to determine the process responsible for the decrease in peak immune cell concentration at small initial patch sizes.

3.1. Not just a rescaling problem

It may be tempting to interpret the effect of the initial patch size on the development and outcome of the infection as a rescaling of the system. In effect, one could imagine that each lump of infected cells represents a single infected cell such that the surface area of one epithelial cell corresponds to s sites of the simulation grid. A grid of area A with an initial patch size of s would be equivalent to a grid of area A/s with an initial patch size of 1. This turns out to be an incorrect interpretation, as seen in Fig. 5. This

Time	# inf.	# new inf.
0	1	8
1	9	16
2	25	24
3	49	32
⋮	⋮	⋮
n	$(2n+1)^2$	$8(n+1)$

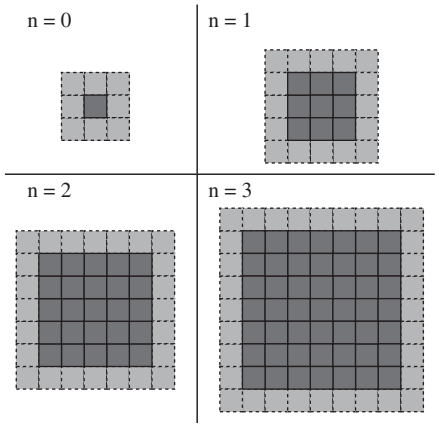

Fig. 2. Evolution of a simplified system where each infected cell infects all of its uninfected neighbours at each time step, starting from a single infected cell. The table shows the number of infected cells and the number of cells that will become infected in the next time step. The figure illustrates the evolution of the system over the first four time steps with infected cells represented in dark grey and the cells which will be infected in the next time step represented in light grey.

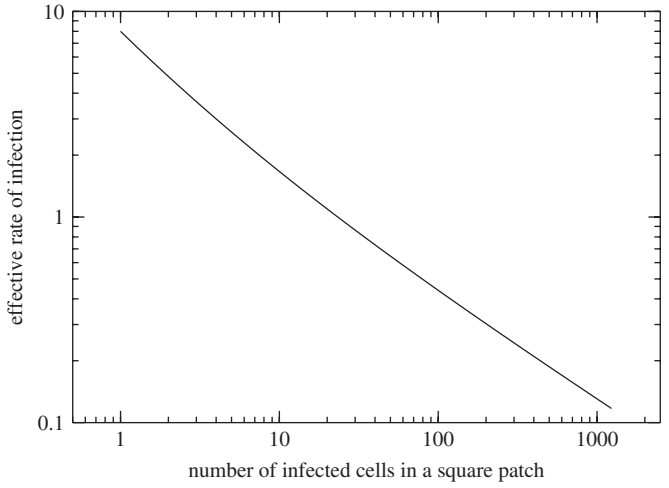

Fig. 3. The effective rate of infection (newly infected cells per infected cell) as a function of number of infected cells in a square patch for the simplified system presented in Fig. 2. The effective infection rate is given by $4/\sqrt{I}+4/I$ where I is the number of infected cells that make up the square patch.

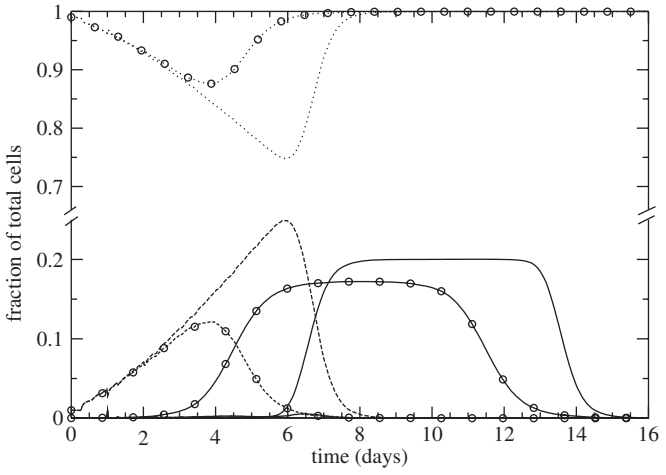

Fig. 4. Proportion of healthy cells (dotted), infected cells (dashed), and immune cells per epithelial cell (full) for two simulations using an initial patch size of $s = 77$. The simulations, whose only difference is the seed for the random number generator, illustrate the differences that can arise for large values of the initial patch size. In this case, early immune detection (lines with circles) of the infection has allowed minimal damage and early recovery, while late detection (lines without symbols) has resulted in a longer infection with a larger number of infected and dead cells.

figure illustrates that one consequence of increasing the number of simulation sites per epithelial cell is an increase in the number of configurations the simulation can be in. For example, this causes the radius of infection sites to grow more slowly, even when the cell-to-cell infection rate is increased so that the rate of increase of infected tissue area is kept constant.

3.2. Occurrence of chronic infection

It is not clear from Fig. 1, but for initial patch sizes larger than 35, a number of simulations result in chronic infection with the fraction of infected cells stabilizing at 2% in all such cases. The occurrence of chronic infection increases for increasing initial patch sizes. This is illustrated in the top left panel of Fig. 6. What causes chronic infections in the case of larger initial patch sizes is the lower effective infection rate, which slows the infection dynamics. If the infection growth is slowed down, the infection takes place over a longer period of time and the immune cells start dying off before the infection is fully cleared. Thus, in the CA model, chronic infection arises when the immune cells' lifespan is shorter than the time scale of the infection. Chronic infections can be prevented by choosing a larger value for δ_M, the lifespan of immune cells, for larger values of s, the initial patch size. For $s = 1232$, there are still occurrences of chronic infection with $\delta_M = 300$ h, but the infections are always cleared for $\delta_M = 400$ h (not shown).

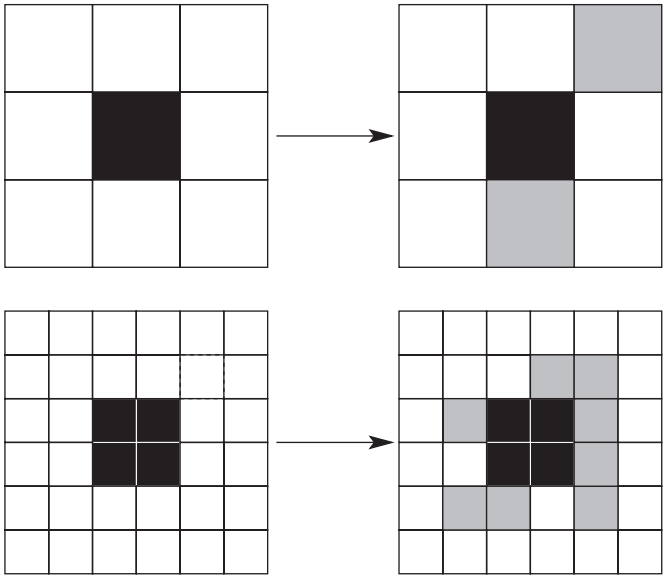

Fig. 5. The comparison of the infection growth pattern for a simulation where each epithelial cell is represented by (top) a single grid site or (bottom) 4 grid sites ($s = 4$). For the infection growth rate to be comparable for the two simulations, the fraction of the grid which gets infected needs to be kept constant such that an infection rate β for an initial patch size of 1 becomes $\beta \cdot s$ for an initial patch size of s. Despite this correction, the infection growth pattern is not equivalent because, for example, the radius of the infection increases faster in the former.

4. Global vs local epithelial regeneration

In the model presented in Beauchemin et al. (2005), the regeneration of dead epithelial cells was implemented as a global process rather than a local process, namely, a dead cell is replaced by a healthy cell with probability $b^{-1} \times \#\,\text{healthy}/\#\,\text{dead}$. See rule 4 of Box 1. This epithelial cell regeneration rule was originally chosen to mimic the replacement of dead cells by basal cells or by cells from inferior layers in the context of an influenza A infection. If one, instead, considers an infection taking place in a tissue composed of a monolayer of cells, a local regeneration rule based on the division of immediate neighbours is more appropriate. In this section, the impact of using the local epithelial cell regeneration rule on the dynamics of the infection is investigated. Local regeneration of epithelial cells is modelled by altering rule 4 of Box 1 so that a dead epithelial cell is replaced by a healthy one only if one of its healthy neighbours divides. Note that for both epithelial cell regeneration rules, division or regeneration is simply the process by which a dead cell is replaced by a healthy cell. If there are no dead cells, nothing happens, no regeneration rule is invoked.

The original global regeneration rule is equivalent to assuming that dead and healthy epithelial cells are homogeneously distributed throughout the simulation grid, which is the way in which epithelial regeneration is implemented in simple ODE models. Comparing the two regeneration rules allows us more insight into the effect of the spatial distribution of cells on localized infection dynamics. The results of simulations comparing the global to the local epithelial cell regeneration rules are shown in the left column of Fig. 7. The top left panel shows the original model with the global epithelial cell regeneration rule, as presented in Beauchemin et al. (2005), and the bottom left panel shows the same model using the local epithelial cell regeneration rule. Time-lapse images of a section of the simulation grid at various days post-infection for both rules are presented in the first and third rows of Fig. 8. Additionally, the numbers of infected and dead cells at their respective peaks relative to their values in the original CA model introduced in Beauchemin et al. (2005) are presented in Table 1 in the two rows labelled "Newly recruited immune cells placed at random locations"; the other rows will be discussed in Section 5. One can see that the local epithelial cell regeneration rule results in fewer infected cells and, consequently, in the recruitment of fewer immune cells but in more extensive and longer lasting damage to the epithelium compared to the global regeneration rule.

In the CA model, the infection of epithelial cells spreads locally as infected cells infect their healthy neighbours forming growing patches of infected cells. As the infection progresses, infected cells at the core of these patches die as a result of virus toxicity or immune attacks, and leave behind patches of dead cells surrounded by a perimeter of infected cells. Patches of dead cells can no longer harbour infection and thus serve to limit the growth of the infection. With the global epithelial cell regeneration rule, new healthy cells are allowed to emerge in the middle of the pools of dead cells. This allows the infection to rapidly repopulate the patches of dead cells, thus sustaining a high level of infection with minimal epithelial damage.

With the local epithelial cell regeneration rule, the patches of dead epithelial cells can only be repopulated by healthy cells once the immune cells have begun destroying the rings of infected cells that encircle each patch of dead cells, which otherwise act as a barrier isolating healthy cells from the areas that require regeneration. Thus, the greater accumulation of damage that results from the use of the local regeneration rule is a consequence of the spatial constraints imposed on the regeneration process. This finding is in agreement with that of Strain et al. (2002), who reported that for their spatial model of HIV, the infection could only be sustained as a propagating wave when the local rate of cell death was greater than the local regeneration rate, as is the case with our model when using the local regeneration rule for epithelial cells.

4.1. Occurrence of chronic infection

Examination of the results of the local epithelial cell regeneration rules for various initial patch sizes reveals the persistence of infected cells, namely a chronic infection

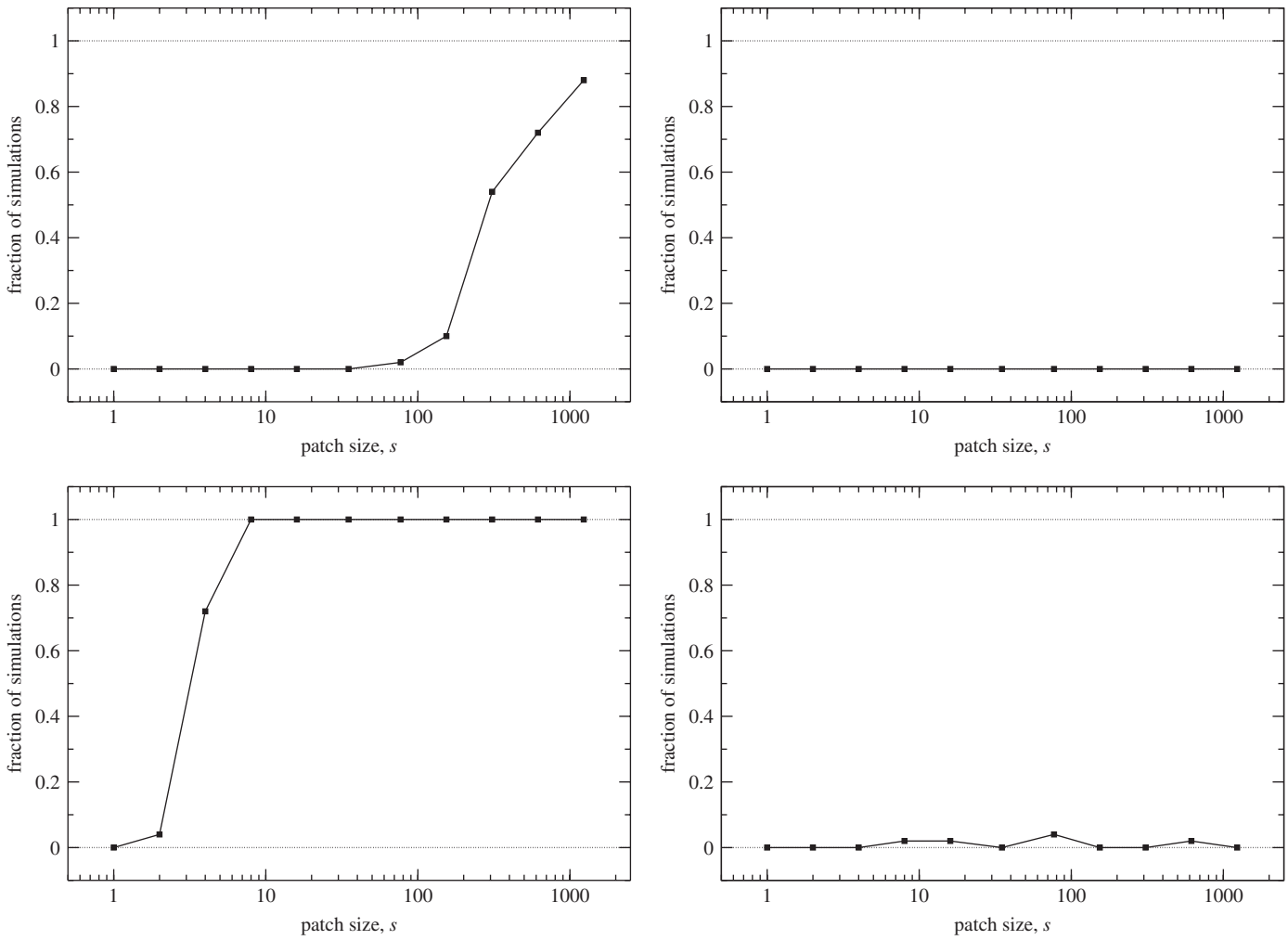

Fig. 6. Fraction of simulations ending in chronic infection as a function of the initial patch size, using the global (top row) or local (bottom row) epithelial cell regeneration rule, with the addition of immune cells at random locations (left column) or at the site of recruitment (right column). The results were obtained by averaging over 50 simulation runs.

stabilizing at approximately 1% of cells infected, for all but an initial patch size of 1. This is illustrated in Fig. 6, where the fraction of simulations ending in chronic infection as a function of the initial patch size for the local epithelial cell regeneration rule is presented in the bottom left panel. The smaller number of infected epithelial cells resulting from the use of the local regeneration rule results in the recruitment of fewer immune cells making it harder to fight the viral infection. Additionally, the organization of the infected cells into circular waves makes it harder for the immune cells to target the infected cells' structures. When infected cells are arranged into patches, an immune cell performing a random walk has better chances of landing on multiple infected sites. When infected epithelial cells organize into rings, as is the case with the local regeneration rule, immune cells performing a random walk will often move off the ring structure and "lose sight" of the infection. Consequently, the smaller number of infected cells and their organization into circular waves facilitates the escape of the infection from immune attacks resulting in a higher incidence of chronic infections than for a global epithelial cell regeneration rule.

5. Immune cells' proliferation rule

The proliferation of immune cells in the model presented in Beauchemin et al. (2005) is such that when an activated immune cell moves onto an expressing or infectious cell, new activated immune cells are added at a rate of $r_M = 0.25$ at a random location on the grid. The addition of immune cells at random locations can be justified biologically by the scenario of immune cells being activated and proliferating in the lymph nodes, travelling to the site of infection, and surfacing at random locations throughout the infected tissue. But immune expansion could instead be modelled by adding new activated immune cells on the site where the recruiting activated immune cell is located, hence mimicking immune cell (T cell, macrophages, etc.) division at the infection site. This scenario could correspond to immune cells being activated in the lymph nodes, but

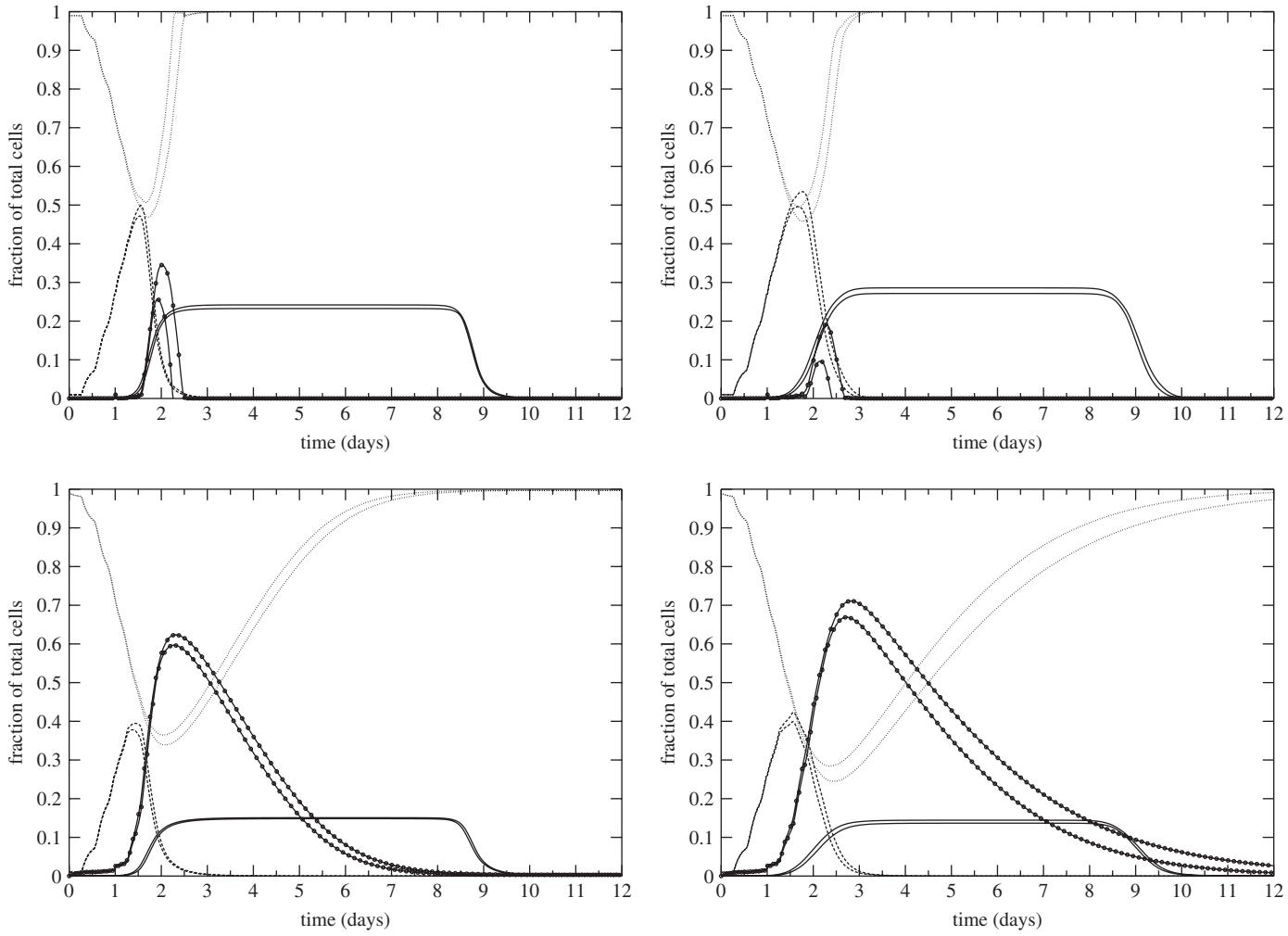

Fig. 7. The effect of a global (top row) or local (bottom row) epithelial cell regeneration rule with the addition of immune cells at random sites (left column) or at the site of recruitment (right column) on the behaviour of the CA model. Simulation results averaged over 50 simulation runs for an initial patch size of 1. The paired lines mark one standard deviation and represent the fraction of epithelial cells that are healthy (dotted), infected (dashed), dead (full with circles), as well as the proportion of immune cells per epithelial cells (full). The top left panel corresponds to the original model presented in Beauchemin et al. (2005).

travelling to the site of infection while still undergoing their programmed cycles of divisions.[2] In Fig. 7, the infection dynamics for the addition of immune cells at random locations and at the site of recruitment are compared for the two choices of epithelial cell regeneration rule. Time-lapse images of a section the simulation grid at various days post-infection are presented in Fig. 8 for the two immune cell proliferation rules for both epithelial cell regeneration rules. Additionally, the numbers of infected and dead epithelial cells at their respective peaks for all rules relative to their values in the original model introduced in Beauchemin et al. (2005) are presented in Table 1.

Regardless of the epithelial cell regeneration rule, the addition of immune cells at the site of recruitment results in more infected cells at the peak of the infection than addition at random locations. The addition of immune cells at random locations allows recruited immune cells to surface randomly onto a previously unexplored site and efficiently discover new patches of infection. With the addition of immune cells at the site of recruitment, it takes longer for immune cells to discover new sites of infection as they can only find them by diffusion. Thus, although the discovered infection sites are cleared faster and more efficiently with the addition of immune cells at the site of recruitment, the undiscovered infection sites are allowed to grow for longer, resulting in more infected cells overall.

In contrast, the addition of immune cells at the site of recruitment rather than at random locations has a different

[2]Note that the immune cells of the model are "generic" immune cells. Their killing of expressing or infectious epithelial cell is reminiscent of killer T cells ($CD8^+$ or cytotoxic T lymphocytes). On the other hand, since infection in the model spreads as infectious cells infect healthy neighbours, the killing of such cells has an effect similar to the clearance of virions by the large amount of antibodies secreted by plasma B cells. As such, the immune cells of the model represent the combined action of various components of the immune response rather than immune cells of a particular type.

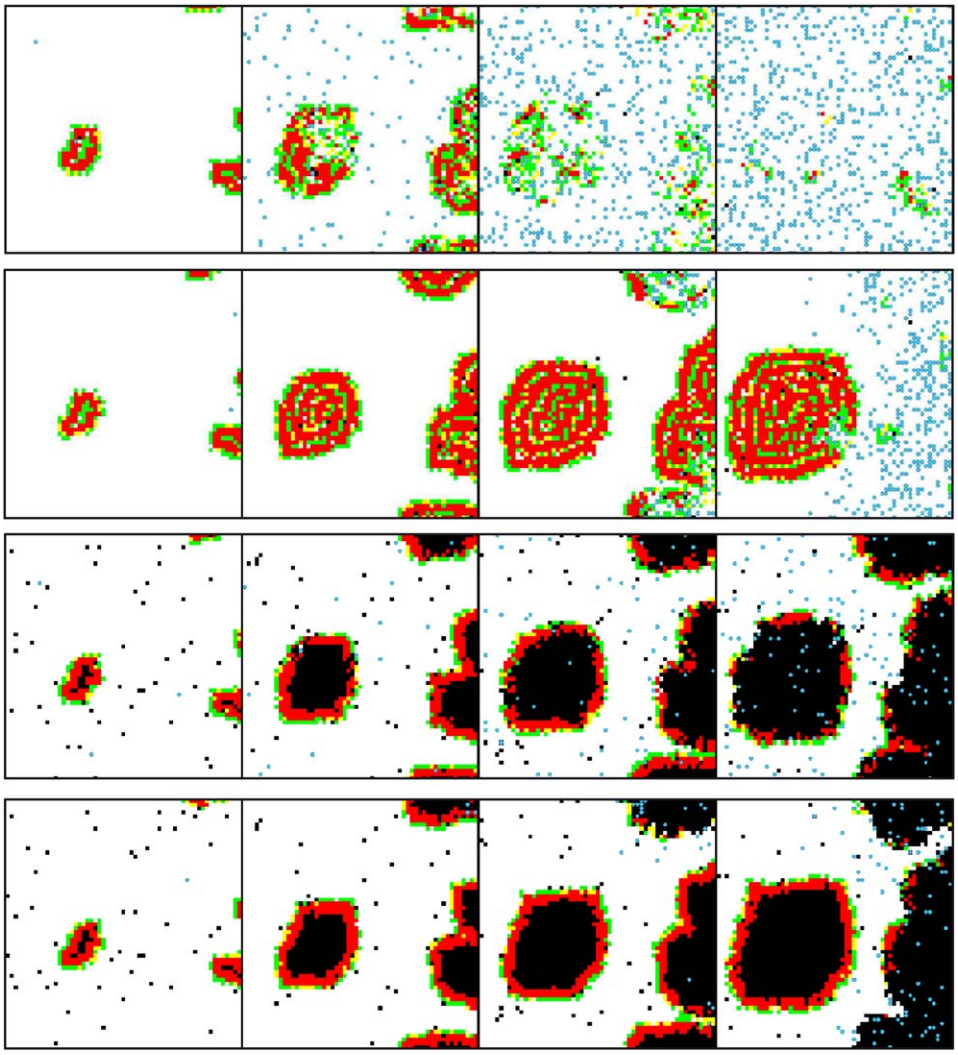

Fig. 8. Time-lapse images of a section of the simulation grid for four simulations obtained using the same parameter values and initial cell distribution at days 1.0, 2.6, 3.5, and 4.4 post-infection from left to right, with an initial patch size of $s = 16$. Each row represents a different rule for the global (top two rows) or local (bottom two rows) epithelial cell regeneration, with the addition of immune cells at random locations (first and third rows) or at the site of recruitment (second and fourth rows). Healthy epithelial cells are white, containing cells are green, expressing cells are yellow, infectious cells are red, and dead cells are black. Immune cells are blue circles. The top row corresponds to the original model presented in Beauchemin et al., 2005.

Table 1
The effects of the epithelial cell regeneration rules and the immune cell recruitment rules on the number of infected and dead cells at their respective peak

Epithelial cell regeneration occurs	Newly recruited immune cells placed at	Maximum infected cells (relative)	Maximum dead cells (relative)
Globally	Random locations	1.0	1.0
	Recruitment site	1.1	0.46
Locally	Random locations	0.80	2.1
	Recruitment site	0.85	2.3

The numbers are relative to their values for the rules of the original model introduced in Beauchemin et al. (2005), namely global epithelial cell regeneration with the addition of immune cells at random locations.

impact on the number of dead cells at the peak for the two epithelial cell regeneration rules. The addition of immune cells at the site of recruitment results in fewer dead cells when combined with the global epithelial cell regeneration rule, but more dead cells when combined with the local regeneration rule. This discrepancy in the effects of the choice of immune cell addition rule for the two epithelial cell regeneration rules can be explained as follows. For the global epithelial cell regeneration rule, the addition of immune cells at random locations allows the infection to grow almost undisturbed while the immune cells slowly populate the grid randomly through recruitment, mainly landing on healthy sites. But when a sufficient number of immune cells have been added, such that new immune cells tend to be placed on infected sites, the destruction of infected cells by immune cells begins and happens very

abruptly. It is this abrupt destruction of infected cells by immune cells that results in the greater number of dead cells seen with the addition of immune cells at random locations rather than at the site of recognition with the global epithelial cell regeneration rule. This also happens when using the local epithelial cell regeneration rule, but in this case the effect is masked by the large increase in cell destruction at undiscovered infection sites. In fact, with the addition of immune cells at the site of recruitment and the local epithelial cell regeneration rule, the undiscovered site are sometimes allowed to grow to such extent that the infection gets cleared by target-cell limitation in those areas.

It might seem at first that the greater number of infected cells resulting from a non-cytopathic pathogen (as cells are no longer dying from the cytopathic effects of the virus) would result in a very extensive amount of damage at the onset of the abrupt destruction of infected cells. However, with this CA model, this does not happen. The results of setting the infected lifespan to $\delta_I = 4 \times 10^6$ h, which is much longer than the duration of the simulation, were compared with those obtained using the original model presented in Beauchemin et al. (2005) in which $\delta_I = 24$ h. The comparison revealed that lengthening the lifespan of infected epithelial cells does not have a significant effect on the resulting dynamics and does not result in extensive epithelial damage. This is because older infectious cells, regardless of their lifespan, find themselves at the centre of infected patches, and so do not contribute to the infection spread since they do not have healthy neighbours to infect. In the case of short lived infected cells (cytopathic pathogen), for example with $\delta_I = 24$ h, dead infectious cells are replaced with healthy cells which are then re-infected and the configuration of the simulation is essentially unchanged from the case of long lived infectious cells. The only difference is that, in the case of long lived infected cells (non-cytopathic pathogen), the uninterrupted presence of the infectious cells causes slightly more immune cells to get recruited.

5.1. Occurrence of chronic infection

Examination of the runs in which immune cells are added at the site of recruitment rather than at random locations reveals a dramatic decrease in the fraction of simulations ending in chronic infection. The addition of immune cells at the site of recruitment using the global epithelial cell regeneration rule produced no chronic infection in any of the 50 simulations performed for each initial patch size. Using the local epithelial cell regeneration rule, the addition of immune cells at the site of recruitment produced only a handful of simulations resulting in chronic infection, with the fraction of infected cells stabilizing at approximately 0.1% in all cases. This is illustrated in Fig. 6.

The reduction in the fraction of simulations resulting in chronic infection when adding immune cells at the site of recruitment rather than at random locations is easily explained. At high infection levels, the addition of immune cells at the site of recruitment increases the efficacy of the response at the site of recruitment but makes it harder for immune cells to find other sites of infection. This results in a greater number of infected cells. But at low infection levels, immune cells added at random locations will rarely be added at an infection site and are likely to die of old age before they can diffuse to an escaped infection foyer. Thus, the addition of immune cells at random locations is the better strategy for high levels of infection allowing rapid detection of the various infection sites, while addition at the recruitment site is the better strategy for low levels of infection allowing efficient prevention of escape.

6. In the context of influenza A

Influenza is a good example of a spatially localized viral infection. The infection typically takes place in the upper 16 generations of the lungs, and the target cells of the infection, the ciliated epithelial cells which cover the respiratory tract, are fixed in place. In previous work (Beauchemin et al., 2005), the CA model used here was introduced and successfully calibrated to mimic a viral infection with influenza A. Here, I revisit the CA model to explore how the local epithelial cell regeneration rule and the immune cell addition rule affect the agreement between the CA model and the experimental data cited in Beauchemin et al. (2005) for an uncomplicated influenza A viral infection. Note that the typical uncomplicated influenza A infection consists of a tracheobronchitis with the additional involvement of small airways. Air flow in large airways is usually unaltered, but small peripheral airways are often affected. Also, uncomplicated influenza causes little permanent damage in the lung (Wright and Webster, 2001).

Because the target cells of influenza A are fixed, i.e. do not move around in space, it is ultimately the speed of diffusion of the virions over the epithelial layer which determines whether the population of infected cells grows locally around a productively infected cell, or in a more homogeneous manner as the virions quickly spread out over the target area. But since the lifespan of a productively infected cell, the number of virions it produces, their clearance rate, and their diffusion pattern in the cilia-beaten mucus are not well known in the case of influenza A, it is difficult to estimate how far and how quickly the infection spreads.[3] Consequently, it is hard to assess the extent to which the infection process, as implemented in the model, applies to the particular case of influenza A. For example, in Section 3, it was shown that larger patches of

[3]The lifespan of a productively infected cell has been reported as 24 h in Bocharov and Romanyukha (1994), 12 h in Baccam et al. (2006), and 33 h in Möhler et al. (2005). The virion burst size has been reported as 10^3–10^4 in Bocharov and Romanyukha (1994), and 1.9×10^4 in Möhler et al. (2005). The virion clearance rate has been reported as 0.1–0.3 h^{-1} in Baccam et al. (2006), and 0.009 h^{-1} in Möhler et al. (2005).

infection lead to a decreased effective infection rate. But if occasional jumps in viral spread to previously uninfected areas were to occur in vivo, they could keep the effective infection rate high, by giving the infection access to areas where target cells are still plentiful. Nevertheless, there are still some conclusions to be drawn from the results presented above.

Originally, in Beauchemin et al. (2005), the use of a global epithelial cell regeneration rule seemed appropriate to mimic the replacement of dead cells by basal cells or by cells from inferior epithelial layers. But in the particular case of influenza A, the infection targets the airway epithelium which consists of a single layer of cells everywhere except in the trachea (Potter, 2004). Thus, it would seem that a local regeneration rule by which a dead epithelial cell is replaced by a healthy cell only if one of its healthy neighbours divides is more appropriate to model cellular regeneration following a viral infection in the lungs. As it turns out, the use of the local epithelial cell regeneration rule does in fact improve the fit of the CA model to available experimental data. Over the course of an influenza infection, there should be about 10% of cells dead on day 1, 40% on day 2 and 10% on day 5 (Bocharov and Romanyukha, 1994). The global rule results in too fast a regeneration, but the local rule improves the agreement of the number of dead epithelial cells during regeneration.

The local epithelial cell regeneration rule also results in a number of infected cells at the peak of the infection (~40% of the total) which is smaller than that obtained with the global regeneration rule (~50% of the total). Unfortunately, there is no data available to assess whether the reduction in the number of infected cells at the peak of the infection constitutes an improvement of the model or not. The other two existing mathematical models of influenza A, which are ODE models, have arrived at numbers of infected cells at infection peak of 37–66% (Baccam et al., 2006), and 60–80% (Bocharov and Romanyukha, 1994) of the total. Experimental data about the fraction of cells infected at the peak of the infection would therefore be invaluable in discriminating between the different models for influenza A and help determine whether spatial heterogeneity plays a role in the development and outcome of the infection.

Finally, it has been suggested in Baccam et al. (2006) that influenza resolution could be target-cell limited. This means that the infection would die from the lack of new cells to infect, rather than as a result of immune attacks. With the model in its current state, target-cell limitation can occur locally, as seen using the local epithelial cell regeneration rule with the addition of immune cells at the site of recruitment (see Section 5).

In the absence of immune cells, target-cell limitation is such that sites of infection grow undisturbed and as the circular waves of infection meet and annihilate, they leave behind nothing but dead cells. Target-cell limited complete resolution of the infection, without the death of all cells, does not occur in the model because as long as the infection wave encircles the dead epithelial cells, segregating them from healthy cells, regeneration cannot be initiated. It is only once immune cells have started attacking the propagating infection wave, creating breaks where dead cells can be in contact with healthy cells, that epithelial cell regeneration can take place.

Target-cell limited resolution could be explored in the absence of immune cells, for example, if the action of cytokines were included in the model. The various cytokines which get produced during an influenza infection are known to hinder viral replication within infected cells, and confer a certain level of protection from infection in surrounding cells (Bocharov and Romanyukha, 1994; Baccam et al., 2006; He et al., 2004; La Gruta, 2004; Tamura and Kurata, 2004; Schmitz et al., 2005). In the CA model, the cytokine response could be modelled by introducing, for example, an inhomogeneous infection rate or an infection rate that would depend on the number of infectious neighbours. This could be the subject of future research.

7. Conclusion

Here, the CA model introduced in Beauchemin et al. (2005) was used to investigate the effects of the well-mixed assumption on the dynamics of a localized viral infection. It was shown that the distribution of initially infected cells has a great impact on the dynamics of infection. This is because, in the CA model, infectious cells can only infect their immediate neighbours, and when organized in patches, fewer infectious cells have healthy neighbours. This is in line with the findings presented in Funk et al. (2005), where the authors compared the results obtained with the basic viral infection model, (1)–(3), to those obtained with an equivalent spatially explicit model. They remark that the spatial model displays a subdued viral growth rate near the infection peak compared to the non-spatial basic model. Funk et al. (2005) warn that such a discrepancy between the basic viral infection model and the equivalent spatially explicit model can lead to systematic errors in estimating parameters from experimental data around the infection peak. In the CA model presented here, the effective infection rate is also subdued as patches of infectious cells grow. This is because it is only the cells at the edges of these patches that have healthy neighbours to infect and thus can participate in the infection. As patches grow, the perimeter to area ratio decreases and so does the effective infection rate.

It was also demonstrated that the regeneration rule chosen for the replacement of dead epithelial cells by healthy ones can have an important impact on infection dynamics. A global epithelial cell regeneration rule, equivalent to simple ODE models, allows areas of dead cells to be replenished by healthy cells even in the local absence of healthy cells. This repopulation, in turn, allows the infection to move back into the newly replenished area it had previously infected, resulting in a greater number of

infected cells. On the other hand, the slower local regeneration rule, which requires the local presence of healthy epithelial cells, limits the growth of the infection by starving it of target cells and forces the infection to propagate as a thin circular wave. Strain et al. (2002) introduce a spatiotemporal model for the dynamics of HIV in the spleen. Strain et al. point out that the main differences between their spatial model and a mean field approach such as the basic viral infection ODE model (Perelson, 2002; Perelson et al., 1996) arise from the fact that a viral burst only spreads to nearby cells. They also conclude that in a spatial model, infection sustainability is affected by the recovery rate of destroyed target cells, as local cell destruction limits the spread of the infection which can then only be sustained as a propagating wave. Those findings are in agreement with those presented here.

Then, the choices of whether to add immune cells at random locations on the simulation grid, equivalent to simple ODE models, or at the site of recruitment were compared to explore how they affect the dynamics of the infection. It was shown that while addition at random sites permits rapid detection of new infection sites, it makes it harder to avoid infection escape from the immune response. Consequently, random addition of immune cells was found to be a better strategy at high infection levels, while addition at the site of recruitment was the better strategy at low infection levels.

The simulation has also been observed to yield chronic infections for certain rules and patch sizes. It is important to specify that the term "chronic infection" is used here to designate a very small fraction (at most 2%) of infected cells persisting beyond at least 60 days post-infection. At this low level of infection, it is unlikely that patients would be symptomatic. Since the patient's nasal cavities in the absence of symptoms (e.g. runny nose) are dryer, it would be difficult to detect any virus shedding from nasal wash. For this reason, I do not believe that current experimental data for influenza can rule out the possibility of a low-level persistent infection. Of course, if it were in fact the case that a low-level of infection can persist, this could have very interesting consequences for memory maintenance, and could possibly provide a reservoir for epidemic spread and strain maturation. Much more sensitive tests than those currently in use would need to be performed to rule out or confirm this possibility.

Cellular automaton type models (also referred to as agent-based and individual-based models) of host–pathogen dynamics are gaining in popularity. Most often, these spatiotemporal models, such as those developed by An (2001), Edelstein-Keshet and Spiros (2002), Segovia-Juarez et al. (2004), Mallet and De Phillis (2006), and Zorzenon dos Santos and Coutinho (2001), are very specific models aimed at capturing the dynamics of a particular disease to try and further our understanding of the processes involved in that disease. Other works have used spatiotemporal models to specifically investigate the effects of the spatial distribution of agents on the evolution and outcome of infections, and chose to remain more general in their investigation by not considering a particular viral infection (Funk et al., 2005; Louzoun et al., 2001). In Strain et al. (2002), the authors both investigated the effects of space on the dynamics of a viral infection and calibrated their model to a particular disease: HIV. Unfortunately, their model makes the assumption that T cells, the target cells of HIV virus, are fixed in space, an assumption that is not realistic given the known patterns of movement of T cells within lymph nodes (Miller et al., 2002, 2003, 2004a, b; Mempel et al., 2004), and this may adversely affect the results. Here, we have explored the effects of relaxing the well-mixed assumption on the spread of a localized viral infection. We have shown that the spatial distribution of agents does have an impact on the severity, duration, and outcome of such infections. In Beauchemin et al. (2005), the model used here was calibrated for influenza A, and was shown to be accurate enough to quantitatively reproduce the response to an uncomplicated infection with this virus. The applicability of the findings presented here follow from that model.

In the present work, the effect of the spatial distribution of infected cells on the dynamics of the infection arises from the fact that the infection can only spread from one infectious cell to its neighbours. The applicability of the findings presented here largely depends on the accuracy of this assumption, namely whether the infection tends to quickly spread over the tissue or grow locally around infected sites. Nonetheless, I have shown in this paper that a local epithelial cell regeneration rule, where a dead cell is replaced by a healthy cell when one of its immediate healthy neighbour divides, improves the fit of the CA model to experimental data in the case of an uncomplicated viral infection with influenza A.

Whether or not there exist in vivo virus–host systems where the infection grows locally from neighbour to neighbour, such systems do exist in vitro and are used to address questions such as how viral spread is inhibited by cellular antiviral activities (Duca et al., 2001; Lam et al., 2005). The team of Dr. John Yin, at the University of Wisconsin—Madison, have introduced a new assay method which consists of a monolayer cell culture covered in an agar solution, which prevents the diffusion of virions at the surface of the cell monolayer such that the infection can only spread to immediate neighbours (Duca et al., 2001; Lam et al., 2005), as is the case in the CA model used here. By complementing these assay experiments with simulations from the CA model used here, significant questions could be addressed. For example, by testing various hypotheses about the production and spread of interferon, and comparing the results of the CA model to that of the experimental assays, it may be possible to discriminate among various potential mechanisms and extract parameters for those mechanisms, such as rate of production/clearance of interferon. The combination of results obtained through such experimental techniques with the flexibility and simplicity offered by spatial *in silico*

Table A.1
Relationship between the notation used in this document and that of Beauchemin et al. (2005)

Notation in Beauchemin et al. (2005)	New notation	Description
FLOW_RATE	v	Speed of immune cells
IMM_LIFESPAN	δ_M	Lifespan of an immune cell
CELL_LIFESPAN	δ_H	Lifespan of healthy epithelial cells
INFECT_LIFESPAN	δ_I	Lifespan of infected epithelial cells
INFECT_INIT	ρ_C	Proportion of initially infected cells
INFECT_RATE	β	Rate of infection of neighbours
EXPRESS_DELAY	τ_E	Delay from containing to expressing
INFECT_DELAY	τ_I	Delay from containing to infectious
DIVISION_TIME	b	Duration of epithelial cells' division (G1 $\rightarrow$ M)
BASE_IMM_CELL	ρ_M	Minimum density of immune cells per epithelial cell
RECRUITMENT	r_M	Number of immune cells recruited when one recognizes the virus
New parameter	s	Number of lattice sites in a patch of initially infected cells

modelling could lead to great advances in our understanding of host–pathogen interactions.

Acknowledgements

This work was supported in part by MITACS' Mathematical Modelling in Pharmaceutical Development (MMPD) project. Portions of this work were done under the auspices of the U.S. Department of Energy under contract W-7405-ENG-36 and supported by NIH Grant AI 28433 awarded to Dr. Alan S. Perelson. The author also wishes to thank Dr. Kipp Cannon and Dr. Alan S. Perelson for helpful discussions.

Appendix A. Notation

Table A.1 lists the relationship between the notation used in this document and that of Beauchemin et al. (2005).

References

An, G.C., 2001. Agent-based computer simulation and SIRS: building a bridge between basic science and clinical trials. Shock 16 (4), 266–273.

Baccam, P., Beauchemin, C., Macken, C.A., Hayden, F.G., Perelson, A.S., 2006. Kinetics of influenza A virus infection in humans. J. Virol., in revision.

Beauchemin, C., 2005. MASyV: a multi-agent system visualization package, version 0.8. Open source software available online on SourceForge at: http://masyv.sourceforge.net.

Beauchemin, C., Samuel, J., Tuszynski, J., 2005. A simple cellular automaton model for influenza A viral infections. J. Theor. Biol. 232 (2), 223–234.

Bocharov, G.A., Romanyukha, A.A., 1994. Mathematical model of antiviral immune response III. Influenza A virus infection. J. Theor. Biol. 167 (4), 323–360.

Duca, K.A., Lam, V., Keren, I., Endler, E.E., Letchworth, G.J., Novella, I.S., Yin, J., 2001. Quantifying viral propagation *in vitro*: towards a method for characterization of complex phenotypes. Biotechnol. Prog. 17 (6), 1156–1165.

Durrett, R., 1994. The importance of being discrete (and spatial). Theor. Popul. Biol. 46 (3), 363–394.

Durrett, R., Levin, S.A., 1994. Stochastic spatial models: a user's guide to ecological applications. Philos. Trans. Biol. Sci. 343 (1305), 329–350.

Edelstein-Keshet, L., Spiros, A., 2002. Exploring the formation of Alzheimer's disease senile plaques *in silico*. J. Theor. Biol. 216 (3), 301–326.

Funk, G.A., Jansen, V.A., Bonhoeffer, S., Killingback, T., 2005. Spatial models of virus-immune dynamics. J. Theor. Biol. 233 (2), 221–236.

Hagenaars, T.J., Donnelly, C.A., Ferguson, N.M., 2004. Spatial heterogeneity and the persistence of infectious diseases. J. Theor. Biol. 229 (3), 349–359.

He, X.-S., Draghi, M., Mahmood, K., Holmes, T.H., Kemble, G.W., Dekker, C.L., Arvin, A.M., Parham, P., Greenberg, H.B., 2004. T cell-dependent production of IFN-γ by NK cells in response to influenza A virus. J. Clin. Invest. 114 (12), 1812–1819.

La Gruta, N.L., Turner, S.J., Doherty, P.C., 2004. Hierarchies in cytokine expression profiles for acute and resolving influenza virus-specific $CD8^+$ T cell responses: correlation of cytokine profile and TCR avidity. J. Immunol. 172 (9), 5553–5560.

Lam, V., Duca, K.A., Yin, J., 2005. Arrested spread of vesicular stomatitis virus infections in vitro depends on interferon-mediated antiviral activity. Biotechnol. Bioeng. 90 (7), 793–804.

Lloyd, A.L., May, R.M., 1996. Spatial heterogeneity in epidemic models. J. Theor. Biol. 179 (1), 1–11.

Louzoun, Y., Solomon, S., Atlan, H., Cohen, I.R., 2001. Modeling complexity in biology. Physica A 297, 242–252.

Mallet, D.G., De Phillis, L.G., 2006. A cellular automata model of tumor-immune system interactions. J. Theor. Biol. 239 (3), 334–350.

Mempel, T.R., Henrickson, S.E., von Adrian, U.H., 2004. T-cell priming by dendritic cells in lymph nodes occurs in three distinct phases. Nature 427 (6970), 154–159.

Miller, M.J., Wei, S.H., Parker, I., Cahalan, M.D., 2002. Two-photon imaging of lymphocyte motility and antigen response in intact lymph node. Science 296 (5574), 1869–1873.

Miller, M.J., Wei, S.H., Cahalan, M.D., Parker, I., 2003. Autonomous T cell trafficking examined *in vivo* with intravital two-photon microscopy. Proc. Natl Acad. Sci. USA 100 (5), 2604–2609.

Miller, M.J., Hejazi, A.S., Wei, S.H., Cahalan, M.D., Parker, I., 2004a. T cell repertoire scanning is promoted by dynamic dendritic cell behavior and random T cell motility in the lymph node. Proc. Natl Acad. Sci. USA 101 (4), 998–1003.

Miller, M.J., Safrina, O., Parker, I., Cahalan, M.D., 2004b. Imaging the single cell dynamics of $CD4^+$ T cell activation by dendritic cells in lymph nodes. J. Exp. Med. 200 (7), 847–856.

Möhler, L., Flockerzi, D., Sann, H., Reichl, U., 2005. Mathematical model of influenza A virus production in large-scale microcarrier culture. Biotechnol. Bioeng. 90 (1), 46–58.

Perelson, A.S., 2002. Modelling viral and immune system dynamics. Nature Rev. Immunol. 2 (1), 28–36.

Perelson, A.S., Neumann, A., Markowitz, M., Leonard, J., Ho, D., 1996. HIV-1 dynamics *in vivo*: virion clearance rate, infected cell life-span, and viral generation time. Science 271, 1582–1586.

Potter, C.W., 2004. Influenza. In: Zuckerman, A.J., Banatvala, J.E., Pattison, J.R., Griffiths, P.D., Schoub, B.D. (Eds.), Principles and Practice of Clinical Virology, fifth ed. Wiley, New York, pp. 271–297 (Chapter 5).

Schmitz, N., Kurrer, M., Bachmann, M.F., Kopf, M., 2005. Interlukin-1 is responsible for acute lung immunopathology but increases survival of respiratory influenza virus infection. J. Virol. 79 (10), 6441–6448.

Segovia-Juarez, J.L., Ganguli, S., Kirschner, D., 2004. Identifying control mechanisms of granuloma formation during *M. tuberculosis* infection using an agent-based model. J. Theor. Biol. 231 (3), 357–376.

Strain, M.C., Richman, D.D., Wong, J.K., Levine, H., 2002. Spatiotemporal dynamics of HIV propagation. J. Theor. Biol. 218 (1), 85–96.

Tamura, S., Kurata, T., 2004. Defense mechanisms against influenza virus infection in the respiratory tract mucosa. Jpn. J. Infect. Dis. 57 (6), 236–247.

Wright, P.F., Webster, R.G., 2001. Orthomyxoviruses. In: Knipe, D.M., Howley, P.M., Griffin, D.E., Lamb, R.A., Martin, M.A., Roizman, B., Straus, S.E. (Eds.), Fields Virology, fourth ed., vol. 1. Lippincott Williams & Wilkins, pp. 1533–1579 (Chapter 47).

Young, W.R., Roberts, A.J., Stuhne, G., 2001. Reproductive pair correlations and the clustering of organisms. Nature 412, 328–331.

Zorzenon dos Santos, R.M., Coutinho, S., 2001. Dynamics of HIV infection: a cellular automata approach. Phys. Rev. Lett. 87 (16).